Generating the Hopf Fibration Experimentally in Nematic Liquid Crystals

Bryan Gin-ge Chen,[1,2] Paul J. Ackerman,[3] Gareth P. Alexander,[4] Randall D. Kamien,[2] and Ivan I. Smalyukh[3]

[1]*Instituut-Lorentz, Universiteit Leiden, Postbus 9506, 2300 RA Leiden, Netherlands*
[2]*Department of Physics and Astronomy, University of Pennsylvania, Philadelphia, Pennsylvania 19104, USA*
[3]*Department of Physics, University of Colorado, Boulder, Colorado 80309, USA*
[4]*Department of Physics and Centre for Complexity Science, University of Warwick, Coventry CV4 7AL, United Kingdom*

(Received 30 December 2012; published 3 June 2013)

The Hopf fibration is an example of a texture: a topologically stable, smooth, global configuration of a field. Here we demonstrate the controlled sculpting of the Hopf fibration in nematic liquid crystals through the control of point defects. We demonstrate how these are related to torons by use of a topological visualization technique derived from the Pontryagin-Thom construction.

DOI: 10.1103/PhysRevLett.110.237801 PACS numbers: 61.30.Jf, 11.10.Lm, 61.30.Dk

The combination of geometric order, optical response, and soft elasticity of liquid crystals uniquely positions them as an arena to study topology: Boundary conditions on sample walls can obstruct smooth solutions in the bulk, forcing points, lines, and walls of diminished order [1]. In general, these topological defects serve as tools for probing the symmetries of the ground state manifold [2], as fundamental excitations [3], and as potential building blocks for self-assembly [4]. Does topology play a role only in systems with *singularities*? Certainly not; the Skyrmion in two and three dimensions is an everywhere smooth complexion of order that is, nonetheless, topologically protected [5,6]. Similar nonsingular configurations are the origin, for instance, of gapless excitations in the quantum Hall effect and topological insulators [7,8]. In nematic liquid crystals, the ground state manifold is the projective plane $\mathbb{R}P^2$ (the sphere with antipodal points identified), and two- and three-dimensional Skyrmions are labeled by elements of the second and third homotopy groups, $\pi_2(\mathbb{R}P^2) = \mathbb{Z}$ and $\pi_3(\mathbb{R}P^2) = \mathbb{Z}$, respectively. The generator of the latter corresponds to the much-storied ''Hopf fibration'' [9], an allowed texture in the nematic phase [10,11]. This celebrated configuration is distinguished by its beautifully interwoven structure of *preimages*: the set of all points in the material where the orientation takes a particular value $\hat{\mathbf{n}}$ [Fig. 2(b)]. The preimage of every orientation is alike—a simple closed circle in space—and the preimage of every pair of distinct orientations is a pair of *linked* circles, whose linking number is the topological quantity (Hopf invariant) that uniquely identifies the texture. Beyond this, the preimages of every orientation with a fixed z component n_z fit together to fill the surface of a torus, while different values of n_z produce a family of nested tori that fill up all of space.

In this Letter, we demonstrate our ability to controllably generate the Hopf fibration experimentally in cholesteric systems: nematics with a preferential handedness, or twist. Our starting point is the toron configuration depicted in Fig. 1 and described in detail in Ref. [12]. This is a tube of double twist that is wrapped upon itself, its boundary forming a torus. Above and below the ''donut hole,'' there are two point defects, both taking the form of hyperbolic hedgehogs. By manipulating these two point defects, we can create a defect-free texture with the topology of the Hopf fibration as in Fig. 2.

How do we know it is the Hopf fibration, and how does the topology work out to render this result? We present a representation of the three-dimensional topology of nematics on a set of two-dimensional surfaces based on the Pontryagin-Thom construction [13,14] which we now briefly sketch. This method is a three-dimensional generalization of the use of crossed polarizers to study schlieren textures in two-dimensional samples with the director taking values in $\mathbb{R}P^1$ [15] and has much of the flavor of manipulating a complex function by moving its poles and branch cuts around.

Recall that the dark lines in a schlieren texture mark those regions where the director is along one of the two polarizer directions. Continuity ensures that the dark lines only end on point defects, and topology ensures that an even number of dark lines emanate from each point defect. We can abstract this slightly by considering just one of the polarizer directions, thus seeing only half the dark lines; note that, in either case, each line carries an arbitrarily chosen yet *globally* consistent orientation so that the lines point from positive to negative defects.

This two-dimensional construction has a natural generalization to three dimensions. We first pick a probe direction $\hat{\mathbf{p}} \in \mathbb{R}P^2$. Next we draw the surface $\Sigma_{\hat{\mathbf{p}}} \in \mathbb{R}^3$, on which the director is everywhere *perpendicular* to the probe, $\hat{\mathbf{p}} \cdot \hat{\mathbf{n}} = 0$. We are therefore looking at the preimage of a curve $\hat{\mathbf{p}}_\perp$ in $\mathbb{R}P^2$, the ''equator'' if $\hat{\mathbf{p}}$ were the ''North pole.'' Were we to look for the preimage of $\hat{\mathbf{p}}$, we would generically only get a curve, and, more problematically, we could get the empty set for a nontrivial texture. The surface construction, however, neatly generalizes the two-dimensional case. The boundaries of any surface are topological defects: A line boundary is the location of a disclination line, carrying the $\mathbb{Z}_2$ charge associated with

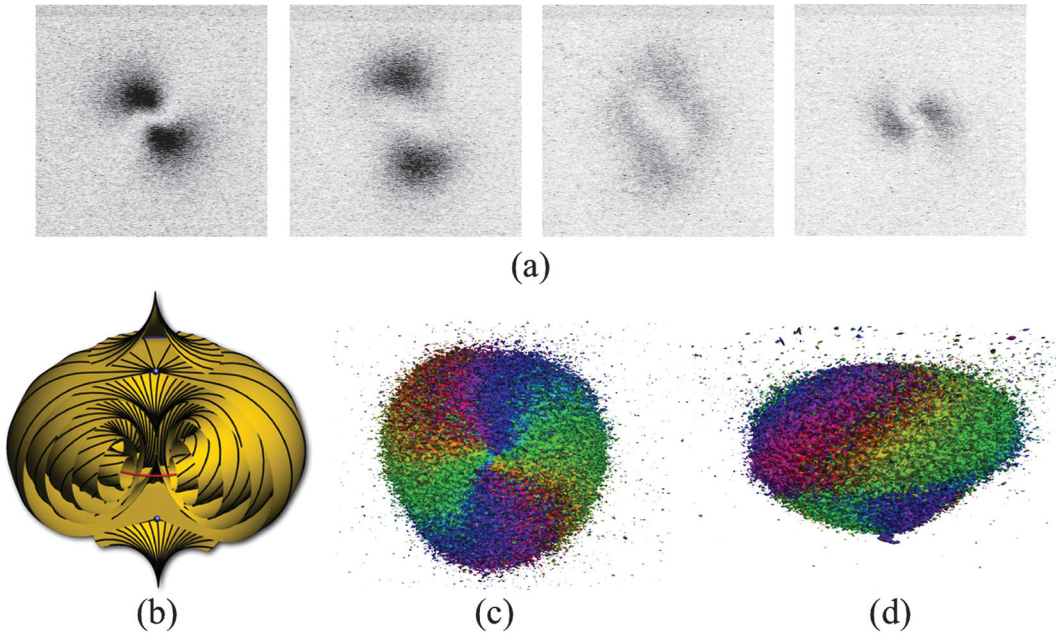

FIG. 1 (color). (a) Selected 3PEF-PM images from an image stack—the images are 16 μm wide and approximately 4 μm apart in the z direction. (b) The toron texture from Ref. [12]. The axis of symmetry of this structure is perpendicular to the substrate. (c) Top view, (d) side view: the "Pontryagin-Thom" surface constructed from this image stack. Despite the considerable noise, the robustness of this method allows us to recognize the nontrivial topology of the texture as the winding bands of color meeting at the two hedgehog defects on top and bottom.

$\pi_1(\mathbb{R}P^2)$, while a point boundary, i.e., a hole in the surface, carries a $\mathbb{Z}$ charge associated with $\pi_2(\mathbb{R}P^2)$. To illustrate, the surface $\Sigma_{\hat{\mathbf{z}}}$ for a toron is shown in Figs. 1(c) and 1(d). It is the set of all points in the material where the director is perpendicular to $\hat{\mathbf{z}}$ and forms a surface that connects the two point defects at the "top" and "bottom" of the toron.

The surfaces, however, do not carry enough information to determine the point charges. In order to capture this information, we must add an additional piece of information to the surface, namely, the direction of the director in $\Sigma_{\hat{\mathbf{p}}}$. We represent this pictorially through a color wheel, ranging from red to violet—through orange, yellow, green, blue, and indigo—as the director rotates by π. We pass through the color wheel a second time if the director rotates by 2π, as it does, for instance, in $\Sigma_{\hat{\mathbf{z}}}$ for the standard radial hedgehog shown in Fig. 3. In fact, since all point defects in a uniaxial nematic can be oriented [16], the usual $\hat{\mathbf{n}} \rightarrow -\hat{\mathbf{n}}$ symmetry does not come into play, and the director always rotates through the color wheel an even number of times, that is, by a multiple of 2π. As a result, a point defect of charge $p \in \pi_2(\mathbb{R}P^2)$ will have a winding of $2p\pi$, or will cover the color wheel $2p$ times, providing a unique identification of point defects in nematics. Thus, looking at the toron in Figs. 1(c) and 1(d) again, the surface $\Sigma_{\hat{\mathbf{z}}}$ is colored as described, and about each point defect there is a twofold winding of the full color wheel, identifying them as carrying unit charge.

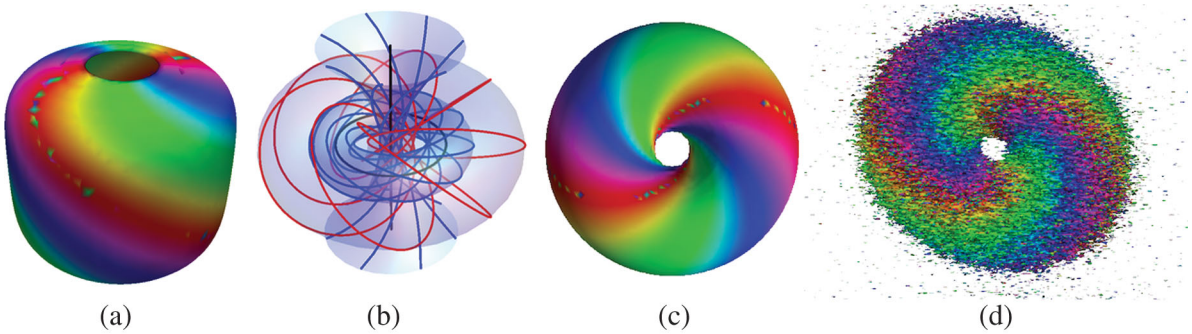

FIG. 2 (color). (a) A simulation of a toron in which the point hedgehogs are replaced with disclination loops. (b) Flow lines of the famous Hopf fibration. (c) The preimage surface of the Hopf fibration, which one can get from (a) by bringing together the two disclination loops through the center of the spool. (d) An experimental image of the same texture.

(a) (b)

FIG. 3 (color). (a) A schematic of a hedgehog-antihedgehog pair; far away, the color is constant, and hence the configuration is topologically trivial. Viewed from below, the handedness of both color wheels changes, illustrating the global sign ambiguity. (b) The same pair of defects moved one on top of the other with the surface bent around. We might think the two defects are of the same sign due to the color rotations if we did not have the surface normal keeping track of the relation to the global base point.

There is an important constraint on the colors that may paint the preimage. The neighborhood of the preimage $\Sigma_{\hat{\mathbf{p}}}$ must admit a continuous map to the ground state manifold [13], and the neighborhood of $\hat{\mathbf{p}}_\perp \in \mathbb{R}P^2$ is a Möbius strip M, a line bundle over the equatorial circle. This means that the normal vectors to points in $\Sigma_{\hat{\mathbf{p}}}$ are mapped continuously to points of M lying "above" the points of the base circle. Since one turn through the color wheel is half a trip through M, the image of the surface normal on any path in $\Sigma_{\hat{\mathbf{p}}}$ whose image in $\mathbb{R}P^2$ wraps the equator once will reverse sign. This extra structure forces every closed curve on $\Sigma_{\hat{\mathbf{p}}}$ to have an even color winding, so that the image of the surface normal in M can be continuous.

Finally, it can be shown that this representation is faithful; that is, up to continuous deformations (homotopy), no information is lost, and the original texture can be reconstructed from the representation we present here [14]. To be more precise, homotopies of the original three-dimensional texture not only induce deformations of the colored surfaces but also may cause the surfaces to merge together along same-colored points or split off new ones (mathematically, such moves are called "bordisms") and vice versa. A key theoretical technique of this Letter is thus exploiting this equivalence: Complicated homotopies of *three-dimensional* nematic configurations can be visualized by simply manipulating these *two-dimensional* surfaces.

In the experiments, we used nematic LC ZLI 2806 doped with the chiral agent CB15 to obtain cholesteric pitch P of interest according to the relationship concentration of CB15 $C = 1/(hP)$, where $h = 5.9\ \mu\text{m}^{-1}$ is the helical twisting power of the used combination of the nematic host and chiral additive. The used cholesteric mixture had $P = 20\ \mu$m to match the thickness of the used capillary d so that $d/P = 1$. A rectangular capillary with a $20 \times 200\ \mu$m cross section was treated for vertical surface boundary conditions by infiltrating it with a 0.1 wt% aqueous solution of a surfactant [3-(trimethoxysilyl) propyl]octadecyldimethylammonium chloride and then evaporating the solution by heating it to 90 °C and keeping it at this temperature for about 30 min. The cholesteric mixture was then heated to isotropic phase at 80 °C and infiltrated to the capillary to avoid filling-induced defects. Various twist-stabilized localized structures in an initially unwound frustrated cholesteric LC were formed through the use of holographic optical tweezers [17] built around a spatial light modulator and a cw laser operating at 1064 nm. Both of the structures described here (torons and Hopf fibration) have an axial symmetry axis which aligns perpendicular to the substrates. Laser beams of power less than 50 mW were focused and spatially steered in 3D within the sample. We have used 10X–100X microscope objectives with numerical apertures ranging within NA = 0.1–1.4 for optical generation.

Imaging of the samples utilized three-photon excitation fluorescence polarizing microscopy (3PEF-PM) [18] integrated with holographic optical tweezers into a single optical setup built around the same inverted optical microscope IX-81 (Olympus). The optical technique of 3PEF-PM [18] is noninvasive, does not require dyes (since the detected fluorescence comes from the LC molecules themselves), and enables the imaging of director fields in 3D. The nonlinear three-photon absorption process gives rise to a $\cos^6\beta$ orientational dependence of the fluorescence signal, where β is the angle between the probing light's linear polarization and the director. The inherent z resolution (along the microscope's optical axis) associated with the nonlinear process allows for optical sectioning and reconstruction of 3D images of the director field. Three-dimensional 3PEF-PM images for four linear polarizations are used to generate a representation in PARAVIEW [19].

Whereas schlieren textures in thin cells give directly the Pontryagin-Thom construction for (quasi-)two-dimensional nematics, the analogous colored surfaces of three-dimensional textures are not an automatic output of any current imaging technique. These surfaces can be extracted easily from knowledge of the director field, which can in turn be obtained from confocal microscopy [20,21] or polarizing-mode nonlinear optical microscopies such as 3PEF-PM, coherent anti-Stokes Raman scattering microscopy [22], and stimulated Raman scattering microscopy [23]. To construct this surface, we take intensity data from confocal slices, polarized at four different angles $\pi/4$ apart in the xy plane (E_0^2, $E_{\pi/4}^2$, $E_{\pi/2}^2$, $E_{3\pi/4}^2$). The Stokes parameters I, Q, and U are

$$I = \frac{1}{2}(E_0^2 + E_{\pi/4}^2 + E_{\pi/2}^2 + E_{3\pi/4}^2), \tag{1}$$

$$Q = E_0^2 - E_{\pi/2}^2, \tag{2}$$

$$U = E_{\pi/4}^2 - E_{3\pi/4}^2. \tag{3}$$

Writing $\hat{\mathbf{n}} = [\sin\theta\cos\phi, \sin\theta\sin\phi, \cos\theta]^T$ and taking the electric field amplitude to simply be proportional to the local electric anisotropy tensor, we find that $I \propto J\sin^n\theta$ and

$Q/U = \tan(2\phi)$, where J is the amplitude of the signal. Here n is an exponent depending on the imaging modality; $n = 4$ for the case of fluorescence confocal microscopy [20,21], $n = 6$ for 3PEF-PM with fluorescence detection without a polarizer [18], and $n = 8$ for coherent anti-Stokes Raman scattering polarizing microscopy with linearly polarized detection collinear with the polarization of excitation light. We then assume that we can shift and normalize the calculated I from the data, so that it takes value from 0 to 1 and the nth root of I gives us $\sin\theta$. The shift is justified in this case, as we expect that away from the toron the director is actually normal to the top and bottom surfaces, along the surface normal, and hence $\theta = 0$ there. The angle ϕ then gives us the angle of the polarization projected to the xy plane, and we can reconstruct the director $\hat{\mathbf{n}}$ from θ and ϕ.

To go from this to the colored surface numerically, we reflect the director field so that it lies in the upper half of the sphere; i.e., if $\cos\theta < 0$, we take $\hat{\mathbf{n}} \to -\hat{\mathbf{n}}$. Using PARAVIEW [19], we then view the isocontour with n_z close to zero. Though one might want to take a slice with n_z zero, the nonorientability of the line field makes it difficult to exclude the artificial ''branch cuts'' where any reconstruction assigns adjacent grid points to different branches of $\hat{\mathbf{n}}$, for example, when $\hat{\mathbf{n}}$ happens to be adjacent to a data point of $-\hat{\mathbf{n}}$. The downside of our approach is that what should be one surface at $n_z = 0$ is actually two nearby surfaces $n_z = \pm\epsilon$. Note that all we pick out here are the surfaces of (near) maximum I, so the sixth-root transformation we made above actually makes no difference; all we need is the fact that the regions in the data where I is maximum correspond to regions where the molecules tend to lie in the xy plane.

We analyzed 3PEF-PM images of several chirally doped nematic textures as described. A precise reconstruction of the director field requires a careful analysis of the optical properties of the material. However, this is unnecessary to determine topological features, which are independent of the fine details and depend only on the coarse structure that is preserved under continuous deformation. Thus, even a highly approximate reconstruction of the director will capture all of the topology correctly.

Using these tools, we can robustly identify the topological nature of three-dimensional textures. Returning first to the toron shown in Fig. 1, the surface $\Sigma_{\hat{\mathbf{z}}}$ is a ''football,'' a closed surface with just two points missing, corresponding to the locations of the two point defects and identified by winding singularities of the color. There are no boundaries to the surface and hence no disclinations. However, the point defects can open up into small disclination loops [12], and the surface then looks like the simulation in Fig. 2(a), where the boundary marks the location of the disclination. In either form, with point defects [Figs. 1(c) and 1(d)] or disclinations [Fig. 2(a)], the preimage of any orientation $\hat{\mathbf{n}} \in \hat{\mathbf{z}}_\perp$ corresponds to a single color on the surface (one line lifts to the vector $\hat{\mathbf{n}}$ and the other to $-\hat{\mathbf{n}}$). Thus, the preimage of any orientation is a curve starting at one point defect and ending at the other. This tells us immediately that the configuration is *not* the Hopf fibration. To create the linking of preimages that characterizes the Hopf fibration, we may bring the two ends together to form a closed loop. In doing so, the defects will cancel and the surface $\Sigma_{\hat{\mathbf{z}}}$ close up to form a torus, as shown in Figs. 2(c) (simulation) and 2(d) (experiment). Again, the preimage of any orientation $\hat{\mathbf{n}} \in \hat{\mathbf{z}}_\perp$ corresponds to a single color on $\Sigma_{\hat{\mathbf{z}}}$. These are all closed circles (one for the vector $\hat{\mathbf{n}}$ and the other for $-\hat{\mathbf{n}}$), and it can be seen directly that each color links every other once in exactly the manner that typifies the Hopf fibration. Thus, by bringing together the two disclination loops through the center of the spool, we have created a degree-one Hopf fibration starting from the toron. Seeing this move directly from the three-dimensional textures in Figs. 1(b) and 2(b) is much more of a challenge.

Experimentally, the transition between the structures can typically be induced by bringing the focused Gaussian laser beam and ''massaging'' (perturbing) the peripheral part of the toron containing the looped double-twist cylinder, but this can occasionally also happen spontaneously. Both structures can be generated from the initial uniform homeotropic state by rapidly moving the focused Gaussian beam along a circle of diameter comparable to that of the double-twist cylinder in the toron.

In closing, we note that this graphical representation immediately makes clear a number of often subtle issues in the description of defects in nematics [16]. First, we can see how the relative charges of two defects depend upon a base point: In this representation, a positive point defect will have a counterclockwise-rotating color wheel, while a negative point defect will have a clockwise-rotating color wheel when we look from above. Were we to look at the same surface from below, however, the handedness of the rotations flips. This corresponds to the global ambiguity in choosing charge associated with the two choices of lifting $\mathbb{R}P^2$ to S^2. It follows that looking at two pieces of surface in the vicinity of two defects does not allow the calculation of their relative degree—one surface must be used in order to consistently determine the topological charge. Finally, note that these surfaces can end on disclination lines, just as the dark brushes in the schlieren texture can end on disclination points in two dimensions. Importantly, the construction of a colored surface from any given liquid crystal texture captures all of the topological information about the texture and also permits the full director field to be reconstructed, at least up to homotopy. In future work, we will use this method to visualize blue phases and other complex textures. Generalizing to biaxial nematics is another extension worth pursuing.

We acknowledge stimulating discussions with D. Beller, F. Cohen, and R. Kusner. G. P. A., B. G. C., and R. D. K.

were supported in part by NSF DMR05-47230 and a gift from L. J. Bernstein. This research was supported in part by the National Science Foundation under Grant No. NSF PHY11-25915. G. P. A., B. G. C., R. D. K., and I. I. S. thank the KITP for their hospitality while this work was being prepared. B. G. C. thanks the hospitality of the Boulder School in Condensed Matter and Materials Physics, where some of this work was completed.

[1] M. Kléman, *Points, Lines, and Walls* (Wiley, New York, 1983).
[2] N. D. Mermin, Rev. Mod. Phys. **51**, 591 (1979).
[3] J. M. Kosterlitz and D. J. Thouless, J. Phys. C **6**, 1181 (1973).
[4] D. R. Nelson, Nano Lett. **2**, 1125 (2002).
[5] T. H. R. Skyrme, Nucl. Phys. **31**, 556 (1962).
[6] N. S. Manton and P. M. Sutcliffe, *Topological Solitons* (Cambridge University Press, Cambridge, England, 2004).
[7] C. L. Kane and E. J. Mele, Phys. Rev. Lett. **95**, 146802 (2005).
[8] D. J. Thouless, M. Kohmoto, M. P. Nightingale, and M. den Nijs, Phys. Rev. Lett. **49**, 405 (1982).
[9] H. Hopf, Math. Ann. **104**, 637 (1931).
[10] Y. Bouligand, J. Phys. (Paris) **35**, 959 (1974).
[11] Y. Bouligand, B. Derrida, V. Poénaru, Y. Pomeau, and G. Toulouse, J. Phys. (Paris) **39**, 863 (1978).
[12] I. I. Smalyukh, Y. Lansac, N. A. Clark, and R. Trivedi, Nat. Mater. **9**, 139 (2010).
[13] B. G. Chen, Ph.D. thesis, University of Pennsylvania, 2012.
[14] T. tom Dieck, *Algebraic Topology* (European Mathematical Society, Zürich, 2008), Chap. 21.
[15] A more well-known S^2 variant of this has been used, for instance, to visualize the braiding of Majorana modes in three-dimensional topological insulator-superconductor systems. See J. C. Y. Teo and C. L. Kane, Phys. Rev. Lett. **104**, 046401 (2010).
[16] G. P. Alexander, B. G. Chen, E. A. Matsumoto, and R. D. Kamien, Rev. Mod. Phys. **84**, 497 (2012).
[17] R. T. Trivedi, T. Lee, K. A. Bertness, and I. I. Smalyukh, Opt. Express **18**, 27658 (2010).
[18] T. Lee, R. P. Trivedi, and I. I. Smalyukh, Opt. Lett. **35**, 3447 (2010).
[19] A. H. Squillacote, *The ParaView Guide: A Parallel Visualization Application* (Kitware, Inc., Clifton Park, NY, 2008), 3rd ed. Software available at http://paraview.org.
[20] I. I. Smalyukh, S. V. Shiyanovskii, and O. D. Lavrentovich, Chem. Phys. Lett. **336**, 88 (2001).
[21] I. I. Smalyukh and O. D. Lavrentovich, Phys. Rev. E **66**, 051703 (2002).
[22] A. Kachynskii, A. Kuzmin, P. N. Prasad, and I. I. Smalyukh, Appl. Phys. Lett. **91**, 151905 (2007).
[23] T. Lee, B. Senyuk, R. P. Trivedi, and I. I. Smalyukh, in *Soft Matter*, edited by A. Fernandez De Las Nieves (Wiley-VCH, Weinheim, to be published).